Published in final edited form as:
Proc Combust Inst. 2021 ; 38(1): 1241–1248. doi:10.1016/j.proci.2020.09.022.

Molecular content of nascent soot: Family characterization using two-step laser desorption laser ionization mass spectrometry☆

Hassan Sabbah[a], **Mario Commodo**[b], **Francesca Picca**[c], **Gianluigi De Falco**[c], **Patrizia Minutolo**[b], **Andrea D'Anna**[c,*], **Christine Joblin**[a,*]

[a]Institut de Recherche en Astrophysique et Planétologie (IRAP), Université de Toulouse (UPS), CNRS, CNES, 9 Av. du Colonel Roche, 31028 Toulouse Cedex 4, France

[b]Istituto di Ricerche sulla Combustione, CNR, P.le Tecchio 80, 80125 Napoli, Italy

[c]Dipartimento di Ingegneria Chimica, dei Materiali e della Produzione Industriale - Università degli Studi di Napoli Federico II, P.le Tecchio 80, 80125 Napoli, Italy

Abstract

Molecules constituting nascent soot particles have been analyzed by two-step laser desorption laser ionization mass spectrometry. Three samples have been collected from a slightly sooting ethylene/air premixed flame with the aim to investigate soot composition in the transition from nucleated to just-grown soot particles. Sampling locations have been selected based on the evolution of the particle size distribution along the flame axis. The mass spectrometric results point to a strong evolution of the molecular composition. Just-nucleated soot is rich in polycyclic aromatic hydrocarbons (PAHs) dominated by medium sizes from 18 to 40 carbon atoms but containing sizes as large as 90 carbon atoms. Most abundant PAHs are in the form of *peri*-condensed structures. The presence of a large fraction of odd numbered carbon species shows that pentagonal cycles are a common feature of the detected population. Increasing the distance from the burner outlet, i.e., the particle residence time in flame, leads to an evolution of the chemical composition of this population with a major contribution of carbon clusters including also fullerenes up to about 160 carbon atoms. Our data support a scenario in which large PAHs containing pentagonal rings evolve very efficiently upon thermal processing by a series of dehydrogenation and isomerization processes to form fullerenes. This chemistry happens in the early steps of soot growth showing that carbonization is already active at this stage.

Keywords

Soot; Carbonization; Polycyclic aromatic hydrocarbons; Fullerenes; Laser mass spectrometry

☆Colloquium: SOOT, NANOPARTICLES, PAH AND OTHER LARGE MOLECULES.

*Corresponding authors. anddanna@unina.it (A. D'Anna), christine.joblin@irap.omp.eu (C. Joblin).

Declaration of Competing Interest
None declared.

Europe PMC Funders Author Manuscripts

Europe PMC Funders Author Manuscripts

1 Introduction

Soot nucleation and early growth in flames has been subject of intense discussion for a long time. The elusive nature of the soot formation mechanism is due to the complexity of the involved chemical and physical processes; these include high-temperature pyrolysis and gas-phase oxidation chemistry, polycyclic aromatic hydrocarbon (PAH) formation, particle nucleation followed by particle growth through coagulation/coalescence and heterogeneous surface reactions. Particle agglomeration, in addition to carbonization/dehydrogenation and oxidation reactions, further contributes to the final shape and structure of the generated particles. As a result, soot particles evolve in flames by changing size, chemical composition and structural order.

The term nascent soot refers to the soot particles during the early stages of the formation process [1], which includes just-nucleated (incipient) to just-grown soot particles. In a laminar premixed flame of an aliphatic hydrocarbon, soot nucleates right after the flame front [2], resulting in the formation of a unimodal particle size distribution (PSD) with a maximum number density for particles of 2-3 nm [3–6]. Once formed, incipient soot undergoes size growth via coagulation/coalescence processes and surface chemical reactions with gas-phase molecules. This next step results in the formation of a second, and larger in size, particle mode whose mean diameter increases as a function of residence time [3–6]. During the growing/aging process in flame, soot is known to carbonize, thus resulting in a lowering of H/C ratio down to the very low value of 0.1 typically associated to mature soot [7,8].

Mass spectrometry techniques (*in situ* and *ex situ*) have contributed significantly to our understanding of the chemistry involved in soot formation and growth [9,10]. Laser desorption/ionization (LDI) techniques [11,12], particularly sensitive to PAHs [13], succeeded to give a comprehensive view of the soot molecular composition during the transition from gaseous phase to solid particles. In order to follow the evolution of the molecular constituents of the particles during the early stages of particle transformation, we have performed two-step laser desorption laser ionization mass spectrometry (L2MS) of the nascent soot particles collected from a slightly sooting ethylene/air laminar premixed flame. The study is aimed at shedding light on the molecular content and its variation with evolving chemical and physical conditions.

2 Experimental

2.1 Flame and soot sampling

Soot particles were sampled from an ethylene/air laminar premixed flame stabilized on a McKenna burner. The cold gas velocity was set to 9.8 cm/s (STP) and the carbon to oxygen (C/O) ratio was 0.67. The particle sampling system for on-line and off-line soot analysis has been described in earlier works [3,14,15]. Briefly, soot was sampled from the flame through an orifice (diameter 0.2 mm, thickness 0.5 mm) in a tubular dilution probe (outer diameter 1 cm), positioned horizontally in the flame. The sampled mixture was immediately diluted with N_2 to quench chemical reactions and minimize particle aggregation [5]. For the off-line analysis, a stainless-steel aerosol filter holder containing a 25 mm pure silver membrane

filter (Millipore-AG4502550) was positioned on-line downstream of the dilution tubular probe for soot nanoparticles collection.

2.2 Mass spectrometry analysis

AROMA (Aromatic Research of Organics with Molecular Analyzer) is an experimental setup that combines laser desorption ionization techniques (LDI) to a segmented linear quadrupole ion trap connected to an orthogonal time of flight mass spectrometer (LQIT-oTOF) [16]. A sketch of the AROMA system (Fig. S1) as well as detailed experimental conditions and performances are reported in the supplementary materials. Mass spectrometry data and chemical analysis tools for all the studied samples are made publicly available in the AROMA database: http://aroma.irap.omp. AROMA was successfully used to characterize, with high sensitivity (down to attomole), PAHs molecular distribution in the Murchison meteorite [16]. Recently [17,18], we have shown the ability of AROMA to track the chemical evolution of carbonaceous molecules involved in the formation of cosmic dust analogues produced from a carbon vapor (C, C_2) and in the presence of H_2 or C_2H_2.

For this work, particles collected on the filter have been analyzed using the well-established and optimized two-step laser mass spectrometry (L2MS) scheme. In this scheme, desorption and ionization are clearly separated and optimized in time and space and performed with two different pulsed (5 ns of pulse duration) lasers. During the desorption step, an infrared laser (Nd:YAG at 1064 nm) is focused on the sample with a spot size of 300 μm producing a fluence of desorption E_d 150 mJ/cm^2. As discussed in the supplementary materials, these conditions ensure thermal desorption avoiding ablation and chemistry in the plume. This implies that the detected molecules come from the surface of the particles with contribution from their volume if these particles consist of loosely bound components. Ionization is performed by intercepting perpendicularly the expanding plume of the desorbed molecules using an ultraviolet laser (fourth harmonic of an Nd:YAG at 266 nm). This scheme presents a high selectivity and sensitivity for species that can undergo (1+1) resonance-enhanced multiphoton ionization (REMPI) such as PAHs and fullerenes [19,20]. The used laser ionization fluence is E_i=16 mJ/cm^2.

3 Results and discussion

The evolution of the particle size distributions in number concentrations for the flame herein investigated, measured along the flame at different burner-to-probe separation distances (Z), has been reported in Ref. [15] (Fig. 1). In the present work three different conditions, i.e., different Z, have been selected for soot sampling and characterization via L2MS-TOF, namely 8, 10 and 14 mm, whose corresponding size distributions in volume are reported in Fig. S2 in the supplementary materials. The PSD in volume develops from a single mode with the most abundant particles having a size of 3.5 nm at Z 8 mm, to a bimodal size distribution where in addition to such incipient particle mode a larger mode made of just-grown soot particles with mobility diameter in the range of 5-15 nm is present at Z 10 mm, and finally to a condition in which most of the mass is in the second mode with a maximum corresponding to particles with mobility diameter of approximatively 20 nm at Z 14 mm. It is worth noticing that for this last condition, the PSD is bimodal if plotted in number, with a

first particle mode centered at approximatively 2.4 nm (roughly as the ones measured at 8 and 10 mm). However, this mode is not observable in Fig. S2 because of the very low mass of such particles [3].

The mass spectra of the three soot samples are reported in Fig. 1 for the 100-2000 m/z range. Three different inset zoom graphs are also sketched with different mass ranges. Molecular mass for the incipient soot particles (Z 8 mm) spans over all the studied range, with the most intense peaks falling in the 200-700 m/z range with a mean weighted mass of m/z 447. Several early studies have led to the observations that nascent soot particles are mainly composed by PAHs of moderate size (about the size of ovalene) [14,15,21], a result which is also consistent with other previous mass spectrometric investigations in similar flame conditions [13,22]. Although, the measurements herein presented are in good agreement with these previous observations, they indicate slightly larger value of the mean molecular mass distribution of the aromatic constituents (C_{36} on average); a result however in closer agreement with the recent LD-MS investigation of soot reported by Jacobson et al. [11]. The PAH distribution obtained in our study spans a large size range with detected species up to about 90 carbon atoms. In addition, peaks corresponding to PAHs having an odd number of carbon atoms from C_9 to C_{91} are measured, some with a strong intensity (e.g., $C_{19}H_{11}$, $C_{21}H_{11}$, $C_{23}H_{11}$).

The mass spectrum for soot collected at Z 14 mm exhibits significant differences. The PAH distribution is shifted to lower mass with a mean at m/z 300 compared to m/z 447 at Z 8 mm. In addition, a series of peaks attributed to pure carbon species (C_x) clearly appears. In the low mass range they are found for each carbon atom numbers, e.g., C_9, C_{10}, C_{11} up to C_{21}. This is followed by a jump to C_{30} from which a series starts separated by 2C up to C_{160}. The most intense peaks are found for C_{60} (m/z 720), C_{50}, C_{52} and C_{70}, which suggests that they correspond to fullerenes [23].

C clusters have been reported by Dobbins et al. [24] for high heights above the burner, using LDI in single step with a 266 nm-laser and an irradiance of 1–20 MW/cm^2. Homann [25], has detected fullerenes in premixed low-pressure flames by on line analysis. The author reported that the formation of fullerenes relative to soot can be so low that these species can only be detected with the most sensitive analytical techniques. Our L2MS technique uses a REMPI scheme, which provides very high sensitivity and was also the one used in Homann's experiments [25]. Our detection is not surprising from this point of view. In addition, we report an evolution with increasing Z both in chemical complexity and in molecular families. The data at position Z 10 mm show an intermediate case in which carbon clusters start to be representative in the mass spectrum. We note that Jacobson et al. [11] could not observe these species, possibly pointing to different sampled flame conditions.

It is worth to note, that the overall intensity of the mass spectra lowers as Z increases. This factor is respectively 1.8 and 3.5 for Z 10 and 14 mm compared to Z 8 mm. This likely reflects a change in the molecular components of the particles, which results in a lower production of molecules upon laser desorption as also noticed in our previous study [15]. In addition, a number of 684, 591 and 463 species have been identified for Z 8, 10 and 14 mm

respectively, which shows that the molecular diversity is changing as well. We will discuss in the following that the probed molecules have been subject to processing which favors the most stable species such as fullerenes.

Some chemical species with one or two oxygen atoms have been observed for samples at Z 8 and Z 10 mm. In each sample about 20 peaks of molecules containing oxygen are identified with an average m/z precision <0.01 (see Table S4). The total ion signal from oxygenated compounds represents 1% from the total ion signal at Z 8 and 3% at Z 10 mm. This low level is consistent with LDI-MS measurements of soot extracted from a diffusion flame [11]. One has to be careful though not to translate this number into an abundance ratio due to the bias of our technique. We note though that evidences of few atomic oxygen percentages in nascent soot were observed by photoemission experiments [26].

In order to obtain a more in-depth evaluation of the aromaticity of the molecular constituents of the nascent soot particles we performed the double bond equivalent (DBE) analysis [16] of the species on the bases of the measured mass spectra. The DBE value is defined by DBE $C\#$ – H#/2 $N\#$/2 1 with C#, H# and N#, the numbers of C, H and N atoms inside the molecules. It is representative of the unsaturation level of the molecules and thus corresponds to a direct measure of their aromaticity. More details about DBE are provided in the supplementary materials.

Colored map plots presenting the calculated DBE/C# values as a function of C# are reported in Fig. 2 for the three samples. The color scale is the relative intensity (normalized to the highest peak in the spectrum) of each species in the mass spectrum. At Z 8 mm, the DBE/C# values are mainly distributed below the planar aromatic limit line (green line), based on the classification of petroleum components [27,28]. For a given number of C atoms, a quite narrow distribution of H atoms is measured with a relevant fraction of aromatic molecules having a molecular structure with a number of H-atoms larger than that corresponding to the most *peri*–condensed structure (magenta line). Still all species stay close to this line, which shows that their structures are compact and do not contain much aliphatic bonds. This statement is strictly valid for PAHs containing 6-membered rings only. Indeed, the introduction of 5-membered rings increases the unsaturation. For instance, the formula $C_{24}H_{12}$ can correspond to the most *peri*–condensed structure coronene, but also to a less compact structure with 2 pentagonal rings as imaged by Commodo et al. [15].

Our results differ from those of earlier studies that concluded about the importance of aliphatic components in the PAH population [29] but is consistent with the more recent study of Jacobson et al. [11].

The DBE/C# values, corresponding to the chemical composition of just-grown soot particles at Z 14 mm, mainly stand above the planar aromatic limit showing an increase of the degree of unsaturation and even the formation of structures with very low hydrogen content. Another important change in the molecular composition between Z 14 and Z 8 mm concerns the highest mass range. From C# 50 and above, 326, 185 and 59 species are detected at Z 8, 10 and 14 mm, respectively. These large species are exclusively fullerenes at Z 14 mm, but none of them are fullerenes at Z 8 mm.

The DBE method allows us to segregate the derived molecular formulas into families. We consider the value of DBE/C# 0.9 as the limit of planar aromatics as defined in Ref. [28]. DBE/C# values below 0.9 correspond to aromatic species with less condensed structures, including potential cross-linked aromatics, and/or the presence of aliphatic CH bonds. DBE/C# values above 0.9 and below 1 correspond to less hydrogenated species that we call HC clusters. In addition, we consider a family of C clusters for C#<30 and fullerenes for C# 30 [23] (Table 1).

Our results show that molecular constituents associated with soot particles change in the passage from the first particle mode at 3.5 nm to the second mode at 9 nm (see Fig. S2). The analysis in molecular families suggests a transition in the population from PAHs to HC clusters and even to fullerenes along the flame (Fig. 3). Indeed, when just-grown soot particles are formed, i.e., Z 14 mm, the few large molecules (C# 50) detached from the particles are found in fullerenes indicating that soot transformation is accompanied by a strong dehydrogenation process of large carbonaceous molecules.

To further explore the molecular family change across the particle growing process we have analyzed in more details the DBE/C# vs C# at Z 8 mm and 14 mm as reported in Fig. S3. At Z 8 mm, the dominant PAH species contain C# 20–24 (see Fig. 2) and a typical number of hydrogens of 10 or 12, which points to a dominant population of compact structures and structures with a few pentagonal rings as discussed above for $C_{24}H_{12}$. As C# increases in the PAH species, the number of hydrogens only slightly increases reaching a maximum of 20 for species larger than 40 carbons. This leads to a growth scheme by a global C_2/C_2H addition, which can be obtained by C_2H_2/C_2H addition and hydrogen removal as postulated in the HACA mechanism [30].

The formation of species with an odd number of C atoms is expected to arise from reactivity with oxygen [25] and also addition of C/CH as suggested in [31,32]. These processes can form pentagonal cycles at the periphery of PAHs. An analysis of the odd-numbered species was performed amongst the population of planar aromatics (DBE/C# 0.9). At Z 8 mm, the odd C number species represent 49% of the peak numbers of which 67% are odd H containing species. The latter number is significantly larger than the total of 48% for these species in the sample. This is consistent with odd C containing PAH species with odd H number corresponding to π radicals. The delocalization of the charge in these ions further contributes to their stability. These odd-numbered structures can include both species with pentagonal ring(s) and some made solely of six-membered rings [25]. At Z 14 mm, the odd hydrogen-containing species sum up to 48% of all the intensity but up to 70% when only odd C containing species (44% of the population) are considered. These numbers appear to be consistent with the value at Z 8 mm suggesting that π radicals constitute a significant fraction of the molecular population.

Concerning the even C number species, mildly dehydrogenated species are observed at Z 8 mm. For instance, the intensity of $C_{24}H_{10}$ is significant (0.45 that of $C_{24}H_{12}$) The presence of less hydrogenated species is confirmed also for large PAHs (see Fig. S3). For instance, for C# 42, the most compact *peri*–condensed structure would correspond to circumpyrene ($C_{42}H_{16}$). Still species corresponding to a lower number of H, in particular $C_{42}H_{14}$ and

$C_{42}H_{12}$ are observed. Similarly, circumcoronene ($C_{54}H_{18}$) is detected together with $C_{54}H_{16}$ and $C_{54}H_{14}$. At Z 14 mm, the intensity of $C_{24}H_{10}$ is 1.5 times higher compared to coronene and we observe much strongly dehydrogenated species (e.g. $C_{24}H_4$, $C_{24}H_6$).

Pure PAHs are expected to exhibit only minor fragmentation during the analysis with AROMA [16]. We therefore consider that these species which contain less hydrogens are intrinsic to the sample and not formed in our analysis. The addition of C_2 can form pentagonal cycles mainly leading to acenaphthylene-type compounds, which can also be found in dehydrogenated form (1,2-dehydro-acenaphthylene; $C_{12}H_6$). In the Z 8 mm sample the ratio $C_{12}H_6/C_{12}H_8$ is equal to 2.3. This might be an explanation for the large intensity of species with mild dehydrogenation (typically 2H below the H number of the most compact *peri*–condensed structures). The presence of pentagonal rings inside the carbon structure is also expected. $C_{20}H_{10}$, which would correspond to the bowl-shaped coran-nulene molecule, has a similar peak intensity as $C_{20}H_{12}$, which would correspond to the full six-membered rings. Therefore, the observed population with low hydrogen content likely reveals the formation of species containing an increasing number of pentagonal cycles. Structures containing several pentagonal cycles are predicted to be the most abundant structures at high temperatures in thermodynamic equilibrium (e.g. $C_{30}H_{10}$ with 6 pentagonal rings and 5 hexagonal rings as predicted by [33]). These pentagonal structures induce some strain that can be release by closing the structure towards fullerenes [34].

The formation of fullerenes in flames was earlier modeled with a gas-phase chemical network taking into account competition between growth and destruction reactions [33,35]. These involved the formation of pentagonal cycles by chemical reactivity as well as by thermal isomerization at the flame temperatures. Homann [25] suggested that the chemistry can proceed via the formation of aromers. Interestingly, our molecular analysis from just nucleated to the just-grown soot, allows us to isolate two regimes. One in which there is a rich chemistry of PAHs leading to the formation of large PAHs containing pentagonal cycles. Another one in which “carbonization” with a significant hydrogen loss seems to govern the chemical evolution of the large carbonaceous molecules. It is interesting to note that for C#≥50, fullerenes are observed at Z = 14 mm but neither PAHs nor HC clusters.For C#<50, a much larger diversity of species are present with HC clusters spanning all possible H numbers.

The transition from PAHs to fullerenes is an interesting topic in astrochemistry that leads to experimental and modeling work [36,37]. Berné et al. [37] have evaluated in their photochemical model, the possibility to convert $C_{66}H_{20}$ (i.e. circumovalene) into C_{60} fullerene upon irradiation by ultraviolet photons. In this scenario, the formation of pentagonal cycles is expected after that PAH has lost all its hydrogen atoms and the carbon cluster rearranges to fold into a fullerene structure, while loosing C_2 until it reaches the most stable fullerene structure of C_{60}. Although the authors concluded about the viability of such a scenario in astrophysical environments, it relies on reaction rates which are poorly constrained especially the ones concerning the folding process for which there is no experimental data. From this study we can however keep the idea of a precursor “PAH-like” population evolving towards fullerenes by energetic processing. In the oxidative environment of flames, the formation of pentagonal cycles during the chemistry of formation

of PAHs can favor the formation of fullerene precursors. Further dehydrogenation and isomerization processes associated to carbonization would then be the key step controlling the transition towards fullerenes. It is striking that a simple calculation using Fig. 3 suggests that this process is very efficient. From Z 8 mm to Z 10 mm, 1.2 10^5 (arbitrary units) large PAHs have been converted into up to 7 10^3 HC clusters and 1.6 10^4 fullerenes. An additional stock of 8.3 10^4 is available from Z 10 mm to Z 14 mm which would lead proportionally to up to 5 10^3 HC clusters and 1.1 10^4 fullerenes. Assuming a similar detection efficiency for both large HC clusters and fullerenes, we conclude that all these produced HC clusters have been converted into fullerenes. The exact fraction of large PAHs that were converted into fullerenes is difficult to assign because of the unknown relative detection efficiency between both populations. Even without considering the detailed numbers, our work suggests that large PAHs are converted into large HC clusters which efficiently produce fullerenes.

4 Conclusions

The molecular constituents of soot have been analyzed using two-step laser desorption laser ionization mass spectrometry in the transition zone from incipient to just-grown soot particles. Fullerenes only appear in the last stage, which implies that they are not involved in soot nucleation. From the analysis of the obtained mass spectra, we came to the following conclusions:

- Molecular constituents of incipient/just-nucleated soot (particles at Z 8 mm) are mostly planar aromatics, not only *peri*-condensed but also in the form of less compact structures (more H atoms with respect to the most *peri*-condensed PAHs) and of structures containing pentagonal cycles (same number of H atoms or less with respect to the most *peri*-condensed PAHs). A large number of radicals are also detected among these aromatic molecules mainly in the form of odd C# with odd H# corresponding to π radicals.;
- Just-grown soot particles (Z 14 mm) contain a population of H-poorer molecules (less than 49 C#), with a similar fraction of the population in radicals than for incipient soot. From sizes 50 C# and above, only fullerenes are observed;
- The evolution of the molecular families within the nascent soot particle zone suggests an efficient conversion of the large PAH population into fullerenes involving intermediate large HC clusters with very fast evolution. This is consistent with a carbonization scheme in which thermal processing induces a series of dehydrogenation and isomerization processes to form the fullerenes.

Supplementary Material

Refer to Web version on PubMed Central for supplementary material.

Acknowledgements

This work was supported by the PRIN-project 2017PJ5XXX:-“MAGIC DUST”. The research leading to these results has received funding from the European Research Council under the European Union’s Seventh Framework Programme (FP/2007-2013) ERC-2013-SyG, Grant agreement N°610256 NANOCOSMOS.

References

1. Wang H. Proc Combust Inst. 2011; 33:41–67.
2. D'Anna A. Proc Combust Inst. 2009; 32:593–613.
3. Commodo M, De Falco G, Bruno A, Borriello C, Minutolo P, D'Anna A. Combust Flame. 2015; 162:3854–3863.
4. Carbone F, Attoui M, Gomez A. Aerosol Sci Tech-nol. 2016; 50:740–757.
5. Zhao B, Yang Z, Wang J, Johnston MV, Wang H. Aerosol Sci Technol. 2003; 37:611–620.
6. Maricq MM. Combust Flame. 2005; 141:406–416.
7. Dobbins RA. Combust Flame. 2002; 130:204–214.
8. Russo C, Tregrossi A, Ciajolo A. Combust Instit. 2015; 35:1803–1809.
9. Pratt KA, Prather KA. Mass Spectrom Rev. 2012; 31:1–16. [PubMed: 21442634]
10. Pratt KA, Prather KA. Mass Spectrom Rev. 2012; 31:17–48. [PubMed: 21449003]
11. Jacobson RS, Korte AR, Vertes A, Miller JH. Angew Chem Int Ed. 2020; 59:4484–4490.
12. Mathieu O, Frache G, Djebaili-Chaumeix N, et al. Proc Combust Instt. 2009; 32:971–978.
13. Faccinetto A, Desgroux P, Ziskind M, Therssen E, Focsa C. Combust Flame. 2011; 158:227–239.
14. Schulz F, Commodo M, Kaiser K, et al. Proc Combust Inst. 2019; 37:885–892.
15. Commodo M, Kaiser K, De Falco G, et al. Combust Flame. 2019; 205:154–164.
16. Sabbah H, Bonnamy A, Papanastasiou D, Cernicharo J, Martín-Gago J-A, Joblin C. Astrophys J. 2017; 843(34)
17. Martínez L, Santoro G, Merino P, et al. Nat Astron. 2020; 4:97–105. [PubMed: 31934643]
18. Santoro G, Martínez L, Lauwaet K, et al. Astrophys J. 2020; 895:97. [PubMed: 33154601]
19. Ahrens J, Bachmann M, Baum Th, et al. Int J Mass Spectrom. 1994; 138:133–148.
20. Streibel T, Zimmermann R. Annu Rev Anal Chem. 2014; 7:361–381.
21. Adkins EM, Giaccai JA, Miller JH. Proc Combust Inst. 2017; 36:957–964.
22. Öktem B, Tolocka MP, Zhao B, Wang H, Johnston MV. Combust Flame. 2005; 142:364–373.
23. Kietzmann H, Rochow R, Ganteför G, et al. Phys Rev Lett. 1998; 81:5378–5381.
24. Dobbins RA, Fletcher RA, Chang H-C. Combust Flame. 1998; 115:285–298.
25. Homann K-H. Angew Chem Int Ed. 1998; 37:2434–2451.
26. Commodo M, D'Anna A, De Falco G, Larciprete R, Minutolo P. Combust Flame. 2017; 181:1339–1351.
27. Marshall AG, Rodgers RP. Proc Natl Acad Sci USA. 2008; 105:18090–18095. [PubMed: 18836082]
28. Lobodin VV, Marshall AG, Hsu CS. Anal Chem. 2012; 84:3410–3416. [PubMed: 22376063]
29. Cain J, Laskin A, Kholghy MR, Thomson MJ, Wang H. Phys Chem Chem Phys. 2014; 16:25862–25875. [PubMed: 25354231]
30. Frenklach M, Wang H. Symp (Int.) Combust. 1991; 23:1559–1566.
31. Joblin C, Masselon C, Boissel P, de Parseval P, Martinovic S, Muller JF. Rapid Commun Mass Spectrom. 1997; 11:1619–1623.
32. Wornat MJ, Vernaglia BA, Lafleur AL, et al. Symp Int Combust. 1998; 27:1677–1680.
33. Pope CJ, Howard JB. Tetrahedron. 1996; 52:5161–5178.
34. Galuá HÁ. Chem Sci. 2014; 5:2667–2676.
35. Howard JB, Lafleur L, Makarovsky Y, Mitra S, Pope CJ, Yadav TK. Carbon. 1992; 30:1183–1201.
36. Zhen J, Castellanos P, Paardekooper DM, Linnartz H, Tielens AGGM. Astrophys J. 2014; 797:L30.
37. Berné O, Montillaud J, Joblin C. Astron Astrophys. 2015; 577:A133. [PubMed: 26722131]

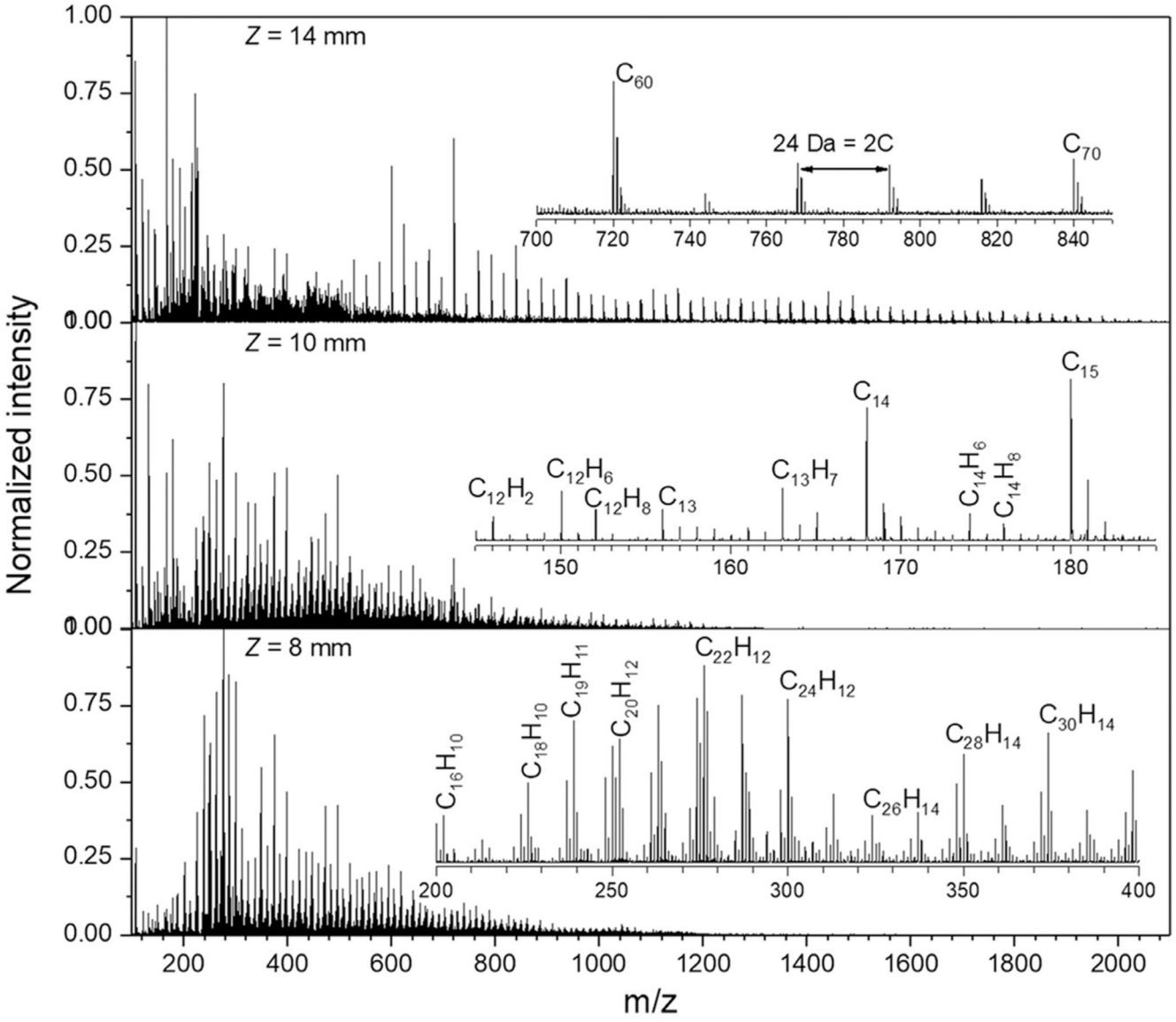

Figure 1. Mass spectra at three burner-to-probe distances, i.e., *Z* 8 mm, *Z* 10 mm and *Z* 14 mm, characteristic of the transition from incipient to just-grown soot particles. Fluences of E_d 150 mJ/cm^2 and E_i 16 mJ/cm^2 have been used for the desorption (1064 nm) and ionization (266 nm) lasers, respectively. Peak annotations are given for corresponding neutral species. Inset zoom graph at *Z* 8 mm presents some of the species detected over the (200–400) m/z range. At *Z* 10 mm the inset zoom graph shows the co-existence of aromatic species with carbon clusters. At *Z* 14 mm the inset zoom graph presents the detection of fullerenes over the (700–840) m/z range. ^{13}C isotopologs are clearly seen in this zoom.

Europe PMC Funders Author Manuscripts

Europe PMC Funders Author Manuscripts

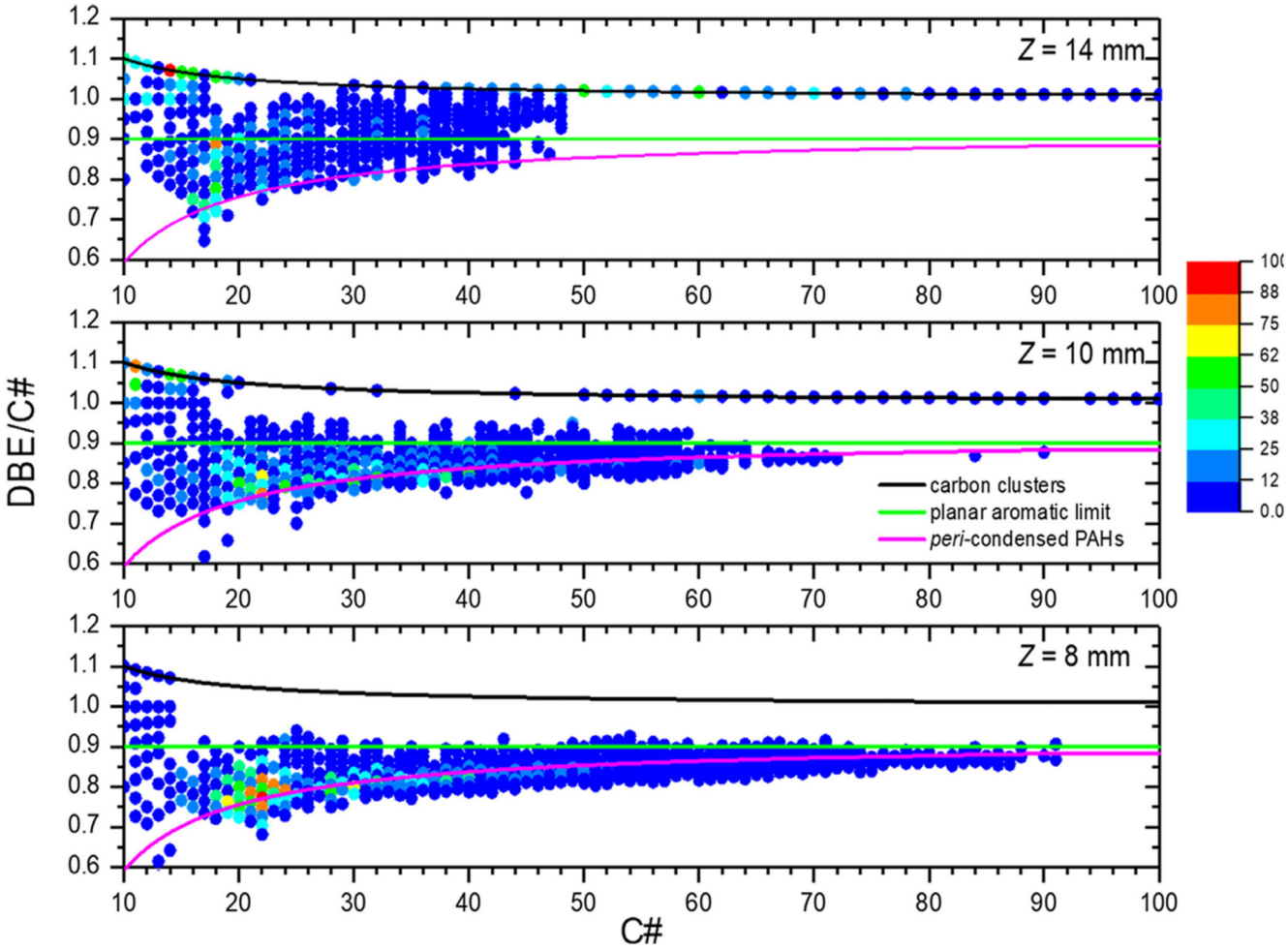

Figure 2. Colored map plots of DBE/C# vs. carbon number (C#) constructed from the molecular formulas which have been derived from the mass spectra of soot sampled at *Z* 8, 10 and 14 mm. The color scale is representative of the relative intensity (normalized to the highest peak in the spectrum) for each identified species. Black line refers to carbon clusters (DBE = C# + 1); green line refers to the planar aromatic limit (DBE = 0.9*C#) [28], and magenta line refers to the purely *peri*-condensed PAHs (most compact structures made of 6-member rings) with DBE = −3.24 + 0.92*C#.

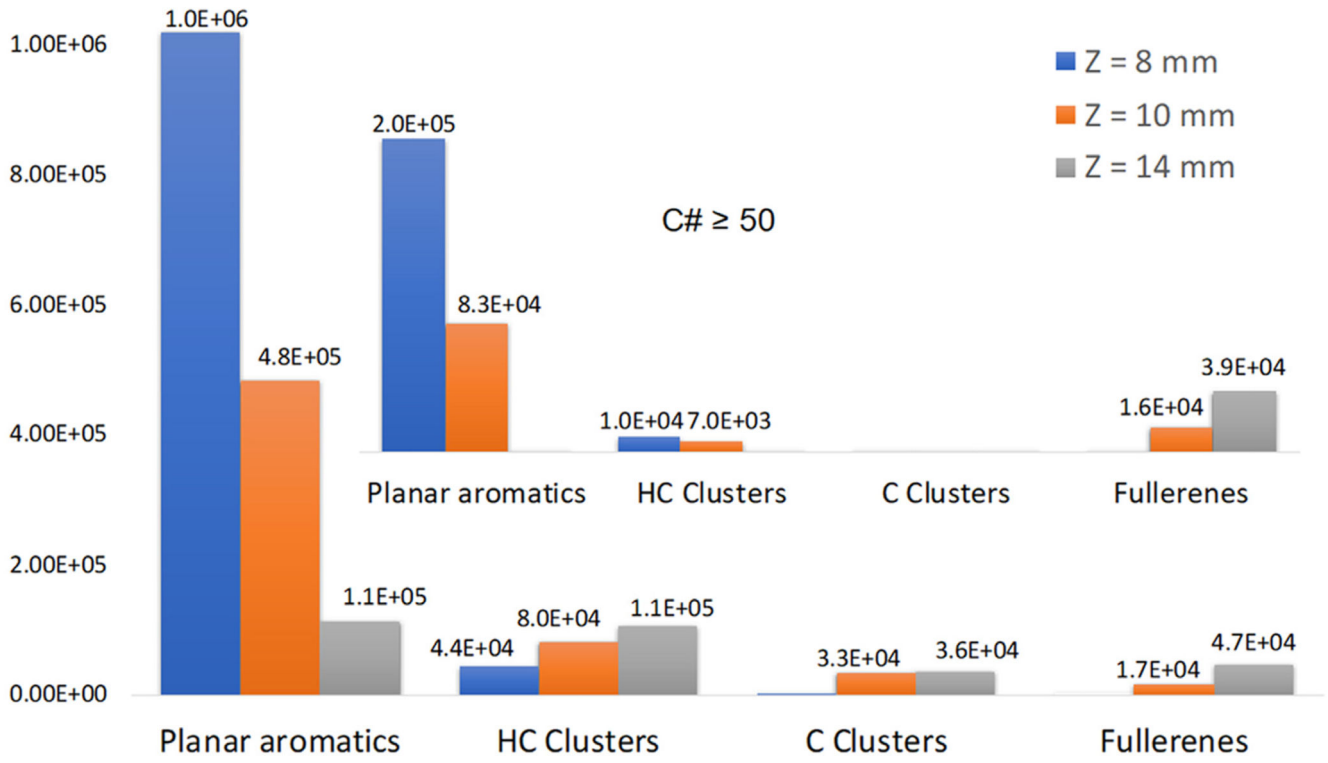

Figure 3. Evolution of the molecular families derived from the mass spectra after DBE analysis.

Europe PMC Funders Author Manuscripts

Europe PMC Funders Author Manuscripts

Table 1

Evolution of the family composition as a function of Z derived from a DBE analysis of the mass spectra in Fig. 1. Sum of relative peak intensities and mean mass (m/z) weighted by peak intensities in parenthesis.

Family composition				
Sample	**Planar aromatics**	**HC Clusters**	**C Clusters**	**Fullerenes**
Z = 8 mm	0.96 (447.30)	0.04 (376.16)	0.00	0.00
Z = 10 mm	0.79 (432.15)	0.13 (338.90)	0.05 (164.22)	0.03 (805.02)
Z = 14 mm	0.38 (300.83)	0.33 (337.36)	0.13 (178.14)	0.16 (874.30)